Journal of Biomedical Optics

SPIEDigitalLibrary.org/jbo

Optical biomarkers for breast cancer derived from dynamic diffuse optical tomography

Molly L. Flexman
Hyun K. Kim
Jacqueline E. Gunther
Emerson A. Lim
Maria C. Alvarez
Elise Desperito
Kevin Kalinsky
Dawn L. Hershman
Andreas H. Hielscher

SPIE

Optical biomarkers for breast cancer derived from dynamic diffuse optical tomography

Molly L. Flexman,[a] Hyun K. Kim,[b] Jacqueline E. Gunther,[a] Emerson A. Lim,[c] Maria C. Alvarez,[c] Elise Desperito,[b] Kevin Kalinsky,[c] Dawn L. Hershman,[c*] and Andreas H. Hielscher[a,b,d*]
[a]Columbia University, Department of Biomedical Engineering, 351 Engineering Terrace, 1210 Amsterdam Avenue, New York, New York 10027
[b]Columbia University Medical Center, Department of Radiology, 630 West 168th Street, New York, New York 10032
[c]Columbia University Medical Center, Department of Medicine, 161 Fort Washington Avenue, New York, New York 10032
[d]Columbia University, Department of Electrical Engineering, 1300 S.W. Mudd, 500 West 120th Street, New York, New York 10027

Abstract. Diffuse optical tomography (DOT) is a noninvasive, nonionizing imaging modality that uses near-infrared light to visualize optically relevant chromophores. A recently developed dynamic DOT imaging system enables the study of hemodynamic effects in the breast during a breath-hold. Dynamic DOT imaging was performed in a total of 21 subjects (age 54 ± 10 years) including 3 healthy subjects and 18 subjects with benign ($n = 8$) and malignant ($n = 14$) masses. Three-dimensional time-series images of the percentage change in oxygenated and deoxygenated hemoglobin concentrations ([HbO_2] and [Hb]) from baseline are obtained over the course of a breath-hold. At a time point of 15 s following the end of the breath-hold, [Hb] in healthy breasts has returned to near-baseline values ($1.6\% \pm 0.5\%$), while tumor-bearing breasts have increased levels of [Hb] ($6.8\% \pm 3.6\%$, $p < 0.01$). Further, healthy subjects have a higher correlation between the breasts over the course of the breath-hold as compared with the subjects with breast cancer (healthy: 0.96 ± 0.02; benign: 0.89 ± 0.02; malignant: 0.78 ± 0.23, $p < 0.05$). Therefore this study shows that dynamic features extracted from DOT measurements can differentiate healthy and diseased breast tissues. These features provide a physiologic method for identifying breast cancer without the need for ionizing radiation. [DOI: 10.1117/1.JBO.18.9.096012]

Keywords: diffuse optical tomography; optical breast imaging; breast cancer; dynamic optical imaging; digital diffuse optical imaging.

Paper 130214R received Apr. 5, 2013; revised manuscript received Jul. 20, 2013; accepted for publication Aug. 2, 2013; published online Sep. 18, 2013.

1 Introduction

From 1975 to 2000, the combination of screening and adjuvant therapy served to reduce the mortality rate due to breast cancer by 24% in the United States.[1,2] Combined with the fact that one in eight women in the United States will develop breast cancer during their lifetime,[1] it is clear that breast cancer screening, diagnosis, and management is a critical issue in women's health. The current gold standard in screening, x-ray mammography, involves painful compression, uses ionizing radiation, and has low specificity leading to unnecessary biopsies. Diffuse optical tomography (DOT) has been considered as an alternative or an adjunct to mammography for identifying and monitoring breast tumors.[3] DOT uses nonionizing near-infrared light to probe tissue noninvasively and has a high sensitivity to breast cancer-relevant chromophores such as hemoglobin, lipid, and water. This modality produces three-dimensional (3-D) maps of the breast chromophores and can image at fast speeds with no need for compression. Studies have shown that DOT has the ability to identify suspicious lesions in the breast,[4–10] differentiate benign from malignant lesions,[4,11] and predict tumor response to therapy.[12–15] The majority of clinical studies to date focus on static imaging of the breast and identify tumors by increased levels of oxygenated hemoglobin concentration ([HbO_2]) and deoxygenated hemoglobin concentration ([Hb]) or differences in the scattering of light through the tumors.

The transient response of tumor vasculature to a stimulus can provide additional information about the tumor characteristics and has been shown in preliminary studies.[11,16–22] Unlike the vasculature of healthy tissue, tumor vasculature is known to be tortuous and disorganized, hyperpermeable, and lack proper vasomotor function.[23] Making use of this fact, these studies looked at the hemodynamic response by applying pressure to the breast and observing differences between the vascular response of healthy and diseased tissues.[16,18,19,22] Other researchers observed that respiratory stimuli cause different optical responses in tumor-bearing breasts as compared with healthy breasts.[17,20] Respiratory stimuli are appealing, because this approach is noninvasive (no injection of foreign substances into the body), does not require painful breast compression, and is easily performed by the patient. However, all respiratory studies to date involved only one or two subjects with no comprehensive investigation into the rich dataset provided by dynamic imaging.

Here, we go beyond these case studies and perform a pilot study involving 21 subjects. We hypothesize that dynamic biomarkers extracted from DOT time-series images, generated during a breath-hold maneuver, can be used to visualize and to characterize breast tumors. Overall, we observed that malignant tumors exhibit a significantly different response to a breath-hold stimulus, as compared with normal tissue, stemming from the notably different vasculature formed by tumor angiogenesis.

*These senior authors contributed equally to this study and manuscript.

Address all correspondence to: Andreas H. Hielscher, Columbia University, Department of Biomedical Engineering, 351 Engineering Terrace, 1210 Amsterdam Avenue, New York, New York 10027. Tel: 212 854 5080; Fax: 212-854-8725; E-mail: ahh2004@columbia.edu

0091-3286/2013/$25.00

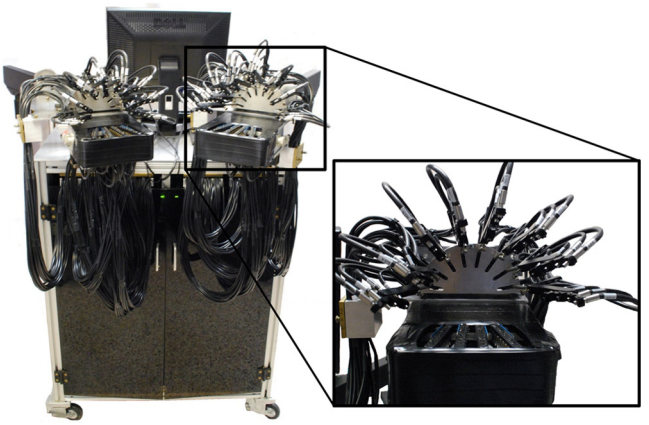

Fig. 1 Photograph of the dynamic diffuse optical tomography (DOT) breast imaging system.

In particular, we found that two dynamic features yield the most statistically significant contrast: deoxy-hemoglobin concentration at a time point of 15 seconds post-breathhold (the mid-recovery point) and the hemodynamic correlation between breasts. In addition, fitting an exponential function to the deoxygenated hemoglobin uptake and washout in the tumor region response provides further insight into hemodynamic changes due to cancer.

2 Materials and Methods

2.1 *Clinical Protocol*

In this study, which was compliant with the Health Insurance Portability and Accountability Act (HIPAA) and approved by the Columbia University Institutional Review Board, informed consent was obtained from 21 subjects. The subjects were instructed to stand in a comfortable position, while the breast interface was brought into contact and adjusted for each breast. The protocol involved 2 to 4 min of baseline imaging, followed by three trials of up to a 30-s breath-hold and a 90-s recovery. During the breath-hold, the subject was asked to avoid a large inhalation and to stop breathing, while maintaining pressure in the mouth and stomach. In the event that the subject could not complete the 30-s breath-hold, she was asked to indicate the end of the breath-hold by opening her mouth (four subjects). Three trials were performed in order to achieve one trial with minimal motion and acceptable breath-hold duration; in most subjects, the second trial was selected for reconstruction.

2.2 *DOT Instrumentation*

All optical measurements were performed using a previously described continuous-wave digital DOT system designed for dynamic measurements of the breast.[24] The system uses four wavelengths of near-infrared light (765, 805, 827, and 905 nm) to illuminate the tissue and can acquire data from 32 sources and 64 detectors per breast with four wavelengths (1.6×10^4 data points per image) at a rate of 1.7 Hz. The system images both breasts simultaneously using a 3-D configuration of optical fibers that surround and make direct contact with the breasts. A photograph of the system and fiber-breast interface is shown in Fig. 1.

2.3 *Image Reconstruction Algorithm*

Three-dimensional reconstructions were performed for the measurement data on a mesh of ~65,000 elements using a recently developed partial differential equation-constrained multispectral imaging method.[24,25] For this study, we use the diffusion approximation to the equation of radiative transfer to describe the light propagation in the breast, a scattering-dominated tissue.

For each subject and each breast, a 50-frame data set (~30 s) acquired immediately prior to the onset of the breath-hold was averaged as a baseline. All chromophores were reconstructed relative to this baseline, and therefore images indicate a change in the concentration of oxy-hemoglobin $\Delta[HbO_2]\%$ or deoxy-hemoglobin $\Delta[Hb]\%$. Any channels with <15 dB signal-to-noise ratio during the baseline period were excluded to avoid numerical instability and artifacts in the final reconstructed image. Further, we assumed typical breast tissue values for the baseline $[HbO_2]$ and [Hb] as 18 and 9 μM, respectively.[26,27] Although these values may not be exact for all subjects, we are most concerned with the dynamic (therefore, relative) changes, and absolute chromophore values are not necessary for that analysis.[28,20] One hundred frame-time sequences corresponding to ~60 s were reconstructed starting from the onset of the breath-hold and lasting through the recovery period.

2.4 *Image Quantification*

All breast data was quantified using an automated MATLAB (Mathworks, Natick, Massachusetts) code to extract the average of a spherical region around the voxel of peak change ($\Delta[Hb]\%$ or $\Delta[HbO_2]\%$). The code automatically identifies the voxel of peak chromophore change for each image frame and takes the average of all voxels that fall within a sphere of radius 1 cm around that peak voxel [our designated region of interest (ROI)]. This technique has previously been used to quantify 3-D DOT images in preclinical studies.[29]

To capture the differences in the overall hemodynamic response, while making use of the simultaneous measurement of optical properties from both breasts, we chose to also look at the correlation coefficient (CC) between the $\Delta[Hb]\%$ in the ROI of the left and the right breast during the 100 frames following the onset of the breath-hold [Eq. (1)].

$$CC = \frac{\sum_{f=1}^{f=100}(\Delta[Hb]\%_{Left} - \overline{\Delta[Hb]\%_{Left}})(\Delta[Hb]\%_{Right} - \overline{\Delta[Hb]\%_{Right}})}{\sqrt{\sum_{f=1}^{f=100}(\Delta[Hb]\%_{Left} - \overline{\Delta[Hb]\%_{Left}})^2(\Delta[Hb]\%_{Right} - \overline{\Delta[Hb]\%_{Right}})^2}} \quad (1)$$

Furthermore, we sought to capture the unique hemodynamic signature of the tumor. To this end, we fitted exponential rise and fall functions to the breath-hold and recovery (60 s total) and minimized the root-mean squared error between the exponential functions and the actual data. Such RC-circuit-like functions are commonly used, e.g., in the field of plethysmography to model hemodynamic responses to cuff experiments,[30] and can in general be expressed as

$$f(t) = f_{sd}\left[t * \frac{(1-e^{-\frac{t}{\tau_r}})}{(1-e^{-\frac{t_{BH}}{\tau_r}})} + f_{su}(t) * e^{-\frac{t-t_{BH}}{\tau_f}}\right], \quad (2)$$

Here, t is the time from the onset of the breath-hold, τ_r is the rise time constant, and τ_f is the fall time constant. For each patient, t_{BH} is automatically determined as the point during the breath-hold where the $\Delta[\mathrm{Hb}]\%$ reaches its maximum. The functions f_{sd} and f_{su} are step down and step up functions, respectively, defined as follows:

$$f_{su}(t) = \left\{\begin{array}{ll} 0, & 0 < t < t_{BH} \\ 0.5, & t = t_{BH} \\ 1 & t > t_{BH} \end{array}\right\} \quad \text{and}$$

$$f_{sd}(t) = \left\{\begin{array}{ll} 1, & 0 < t < t_{BH} \\ 0.5, & t = t_{BH} \\ 0 & t > t_{BH} \end{array}\right\}. \quad (3)$$

All exponential fitting were performed on normalized experimental data in order to characterize the shape of the curve without considering the amplitude of change, and for this reason, Eq. (2) is normalized to unity at time t_{BH}.

2.5 *Study Population*

Dynamic DOT measurements were performed on 21 subjects over the course of 1 year. Three of the subjects were healthy volunteers, while the other 18 had a benign or malignant mass. Thirteen of the 21 subjects were postmenopausal with a mean age of 54 ± 10 years and a mean body-mass index (BMI) of 30 ± 4. Fourteen subjects had a malignant mass in one breast, of which four were invasive ductal carcinomas (IDC), one was invasive lobular carcinoma (ILC), two were ductal carcinomas *in situ* (DCIS), and seven were a combination of IDC, ILC, and DCIS. Three subjects had a benign mass in one breast, and one subject had benign masses in both breasts. Three subjects with a malignant mass in one breast also had a contralateral breast with a benign mass. Of the eight benign masses, one was atypical ductal hyperplasia (ADH), four were fibroadenomas (FA), one was a cyst, one was sclerosing adenosis (SA), and one was unbiopsied. The average mass size was 1.6 cm ranging from 0.1 to 4 cm. Overall, there were $n = 8$ breasts with benign masses and $n = 14$ breasts with malignant masses. Unless explicitly mentioned, all of these breasts were included in our statistical analysis.

All the subjects in this study had prior mammograms for comparison. In most cases, ultrasound and dynamic contrast-enhanced magnetic resonance imaging images were also available and were used to verify the tumor location and size. Table 1 contains a summary of the subjects who participated in the study.

2.6 *Statistical Analysis*

To compare the three groups (healthy breasts, breasts with a benign mass, and breasts with malignant masses), we employed the Holm t-test.[31–33] This test applies an accept/reject criterion to a set of ordered-null hypotheses, starting with the smallest p-value and proceeding until it fails to reject a null hypothesis. The null hypothesis in our case is that there is no difference between the three groups, or in other words that the samples are drawn from the same population. Therefore, we start by calculating the uncorrected p-values with a student t-test for all $k = 3$ pairwise comparisons (healthy-malignant, healthy-benign, and benign-malignant). The resulting p-values are ordered from the smallest to the largest with the smallest p-value considered first in a sequential step-down test procedure. For the j'th hypothesis test in this ordered sequence, the Holm's test applies the Bonferroni criterion[32] until one fails to reject the null hypothesis. Specifically, the uncorrected p-value for the j'th test is compared with $\alpha_j = \alpha_T/(k-j+1)$. For the first comparison, $j = 1$, the uncorrected p-value needs to be smaller than $\alpha_1 = \alpha_T/(k-j+1) = \alpha_T/k$. If the smallest calculated p-value is less than α_1, we reject the null hypothesis, and then compare the next smallest uncorrected p-value with $\alpha_2 = \alpha_T/(k-2+1) = \alpha_T/(k-1)$, etc. With $\alpha_T = 0.05$ (significance level of 95%) we get in our case ($k = 3$), $\alpha_1 = 0.0167$, $\alpha_2 = 0.025$, and $\alpha_3 = 0.05$; and with $\alpha_T = 0.01$ (significance level of 99%), we get $\alpha_1 = 0.0033$, $\alpha_2 = 0.005$, and $\alpha_3 = 0.01$. All p-values subsequently reported in this article should be compared with these α-values for assessing significance. For a more detailed discussion of this approach to multiple group comparisons, see Refs. 31–33.

3 Results

With the onset of the breath-hold, we observe in all subjects an increase in $\Delta[\mathrm{Hb}]\%$ and $\Delta[\mathrm{HbO_2}]\%$ levels in the breast. Upon resuming normal breathing, the $\Delta[\mathrm{Hb}]\%$ and $\Delta[\mathrm{HbO_2}]\%$ levels gradually return to the baseline values. Typically, in breasts with a malignant mass, there is a notable difference in the hemodynamic response over the course of the breath-hold as compared with healthy breasts. As an example, Fig. 2(a) shows the $\Delta[\mathrm{Hb}]\%$ response in the ROI over the course of a 20-s breath-hold and recovery for a 64-year-old subject with a 1.4-cm tumor in the right breast identified as Subject 12 (S12) in Table 1. Although both the healthy left and the tumor-bearing right breasts were imaged during the same breath-hold, their hemodynamic response is markedly different. In contrast, the left and the right breasts of a 63-year-old healthy subject (S3) have nearly identical responses to a 30-s breath-hold [Fig. 2(b)].

3.1 *Mid-Recovery Tumor Visualization*

Figure 3(a) shows DOT coronal slices through the left and the right breast from a 57-year-old postmenopausal woman [identified in Table 1 as Subject 17 (S17)] for multiple time points during the breath-hold and the recovery sequence. The tumor, an invasive ductal and lobular carcinoma located at the 11o'clock position in the right breast, is most visible during the mid-recovery time point (15 s after resuming normal breathing) by a substantial (10%) enhancement in $\Delta[\mathrm{Hb}]\%$ [Fig. 3(b)]. Similarly, one can also observe an increase in $\Delta[\mathrm{HbO_2}]\%$ [Fig. 3(c)], although at only 2%, this increase is smaller than that of $\Delta[\mathrm{Hb}]\%$. The ipsilateral breast [Fig. 3(a), left] shows a more moderate 4% increase in $\Delta[\mathrm{Hb}]\%$ that was typically observed in healthy breasts.

The increase in $\Delta[\mathrm{Hb}]\%$ in the tumor region at the mid-recovery time point is observed across multiple pathologies including IDC, ILC, and DCIS, but not in healthy breasts, as shown in Fig. 4. An enhancing region can be seen in the correct location for each of the cancerous pathologies [Figs. 4(a)–4(d)], but no enhancing regions are visible in the case of a benign pathology [Fig. 4(e)] or in a healthy subject [Fig. 4(f)].

Table 1 Summary of subjects and pathologies.

Subject	Age	BMI	Cup	Pathology	Location[b]	Size[c]
1	41	22.6	C	Healthy Healthy	Left breast Right breast	—
2	61[a]	32.9	DD	Healthy Healthy	Left breast Right breast	—
3	63[a]	31	C	Healthy Healthy	Left breast Right breast	—
4	44	22.4	B	IDC + DCIS	Right 1:00, 5 cm FN	2.7
				Benign (SA)	Left 2:30, 6 cm FN	0.5
5	49	29.2	D	IDC + ILC	Left 3:00, Posterior	1.9
6	70[a]	28.7	DDD	IDC	Right 2:00, 10 cm FN	2.2
7	63[a]	31.5	DDD	IDC	Right 1:30, posterior	3.0
				Benign (cyst)	Left 2:00, 5 cm FN	0.6
8	41	27.4	D	ILC	Right 10:00, posterior	2.6
9	58[a]	28.7	C	IDC + ILC	Left 2:30, 10 cm FN	2.1
10	56[a]	30.2	C	IDC + ILC	Right 9:00 to 10:00	4.0
				Benign (FA)	Left 2:00	0.1
11	63[a]	25.8	C	DCIS	Right 11:00, 5 cm FN	2.2
12	64[a]	26.7	B	IDC + ILC + DCIS	Right 1:00, 3 cm FN	1.4
13	42	43.1	D	IDC +ILC + DCIS	Left 1:30, 13 cm FN	1.3
14	68[a]	32.3	C	IDC	Right upper outer quad[d]	2
15	38	30.4	D	IDC	Right 9 to 10:00, 5 cm FN	1.5
16	58[a]	30.4	C	DCIS	Left 2:00, 6 cm FN	1.8
17	57[a]	28.6	B	IDC + ILC	Right 11:00, 1 cm FN	0.5
18	42	31	DD	Benign (FA)	Left 7:00, 3 cm FN	1
				Benign (FA)	Right 5:00, 8 cm FN	1
19	47	31.4	C	Benign (unbiopsied)	Right 7:30, 5 cm FN	1
20	55[a]	23.2	C	Benign (FA)	Right 6:00, 6 cm FN	0.7
21	61[a]	28.3	DDD	ADH	Left 11:00, 3 cm FN	1.1

[a]The subject is postmenopausal.
[b]Location indicated as a clock face position and a distance from the nipple (FN) in cm as defined by the SEER coding guidelines.[1]
[c]Size of the largest dimension of the tumor (in cm).
[d]Extremely dense breasts—precise location and size not known.

3.2 *Quantification of Mid-Recovery* Δ[Hb]%

To quantify the changes in Δ[Hb]% in the region of the tumor at the mid-recovery time point, we performed a statistic analysis of all subjects. Figure 5(a) shows the average Δ[Hb]% for healthy breasts ($n = 6$), breasts with benign masses ($n = 8$), and breasts with malignant masses ($n = 14$). The values of Δ[Hb]% were calculated by averaging over a 1-cm-radius sphere surrounding the peak Δ[Hb]% in each patient. At the mid-recovery time point, the healthy breasts have almost returned to the baseline (mean $= 1.6\% \pm 0.5\%$), while the malignant regions still have some Δ[Hb]% lingering through the recovery period (mean $= 6.8\% \pm 3.6\%$). The values for breasts with benign masses (mean $= 4.9\% \pm 2.7\%$) fall between the values observed for healthy breast and a breast bearing a malignant mass. There is a significant difference in Δ[Hb]% between healthy breasts and breasts with a malignant mass ($p = 0.0002$) as well as between the healthy and benign breasts ($p = 0.014$), but not

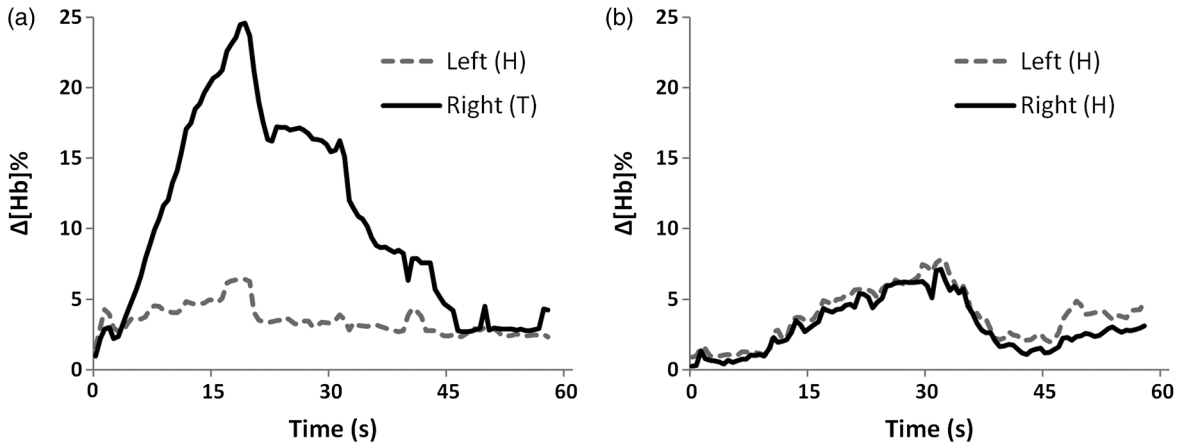

Fig. 2 Percentage change in deoxy-hemoglobin extracted for each three-dimensional (3-D) DOT image frame by taking the average over a 1-cm-radius sphere of peak Δ[Hb]%. Δ[Hb]% is shown over the course of a breath-hold and recovery period for (a) a 64-year-old subject (S12) with a 1.4-cm tumor in the right breast (solid black line) and (b) a 63-year-old healthy subject (S3). In (a), the breath-hold lasted 20 s, while in (b) the breath-hold lasted 30 s.

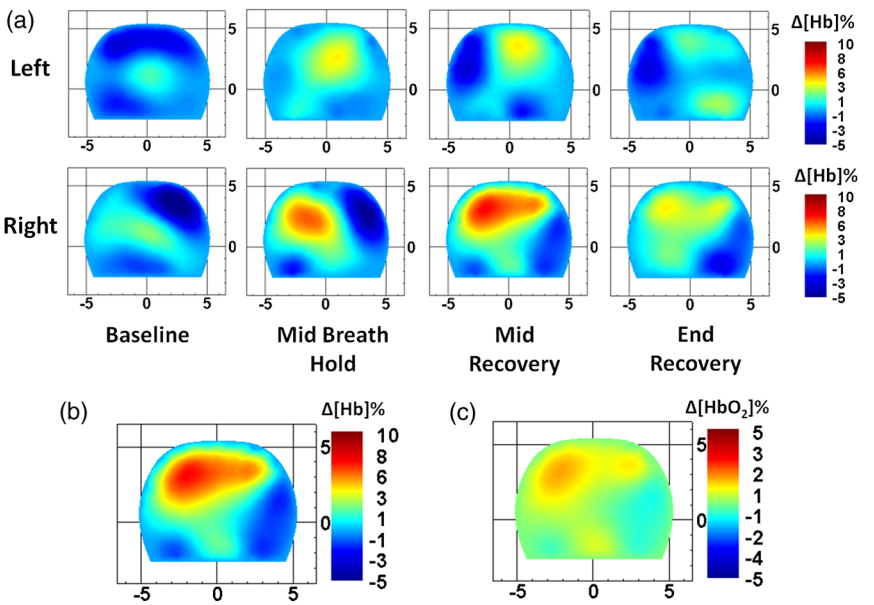

Fig. 3 (a) Coronal slices looking at the Δ[Hb]% in the left (top) and right (bottom) breast at four different time points over the course of the breath-hold: Baseline ($t = 0$ s), mid-breath hold ($t = 20$ s), mid-recovery ($t = 45$ s), and end recovery ($t = 60$ s) There is an invasive carcinoma at 11 o'clock in the right breast (S17), which is most visible during the mid-recovery time point ($t = 45$ s, 15 s after resuming normal breathing at $t = 30$ s). Coronal slices showing (b) Δ[Hb]% and (c) Δ[HbO_2]% demonstrate that while an enhancement of Δ[HbO_2]% is seen in the tumor region, the contrast is not as great as in Δ[Hb]%.

between breasts bearing a benign mass and a malignant mass ($p = 0.19$).

To standardize the technique for better comparison across subjects, we normalized each breast to the maximum Δ[Hb]% in the ROI over the course of the breath-hold in either breast for each subject [Fig. 5(b)]. Similar to the results found in Fig. 5(a), the healthy breasts and breasts with a benign mass have much smaller normalized Δ[Hb]% [mean (healthy) $= 0.17 \pm 0.1$, mean (benign) $= 0.31 \pm 0.22$], while the malignant-mass bearing breasts have a larger fraction of deoxy-hemoglobin remaining in the tumor region at mid-recovery time point [mean (malignant) $= 0.45 \pm 0.27$]. With this normalization, we find that there is a significant difference between the healthy and the tumor-bearing breasts ($p = 0.004$), but not between benign and healthy breasts ($p = 0.12$) or benign and malignant breasts ($p = 0.22$).

3.3 *Correlation Between Breasts*

Subjects with two healthy breasts showed a high correlation between the hemodynamic response to the breath-hold in both the left and the right breasts [mean $(CC_{healthy}) = 0.96 \pm 0.02$]. This correlation is somewhat lower in breasts with a benign mass [mean $(CC_{benign}) = 0.89 \pm 0.02$] and, on average, much lower for breasts with a malignant mass [mean $(CC_{malignant}) = 0.75 \pm 0.23$]. Using the Holm's test, the differences between healthy subjects and patients with benign and malignant masses is statistically significant ($p = 0.010$ and $p = 0.015$, respectively), while the p-value for the comparison of patients with benign and malignant masses is slightly above the 0.05 threshold with 95% significance ($p = 0.060$). (Note that to study the correlation between tumor bearing and healthy breast, we excluded the four patients who had lesions in both breasts.)

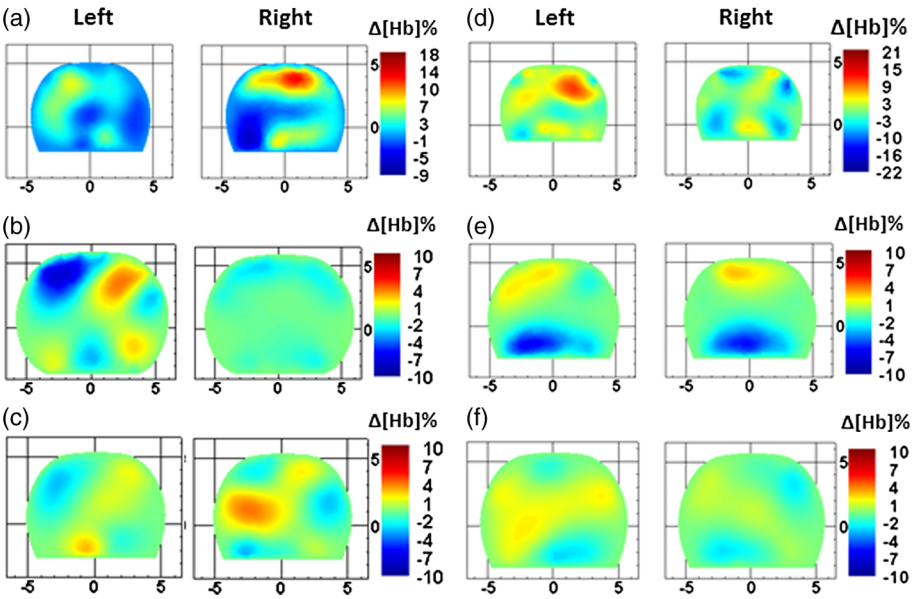

Fig. 4 Coronal slices through the breast showing the Δ[Hb]% for the left and the right breast at the time point 15 s into the recovery period. The cases shown include (a) an invasive ductal carcinomas (IDC) at 1:00 in the right breast (S4); (b) an IDC and invasive lobular carcinoma (ILC) at 2:30 in the left breast (S9); (c) an ILC at 10:00 in the right breast; (d) ductal carcinoma *in situ* at 2:00 in the left breast (S16); (e) atypical ductal hyperplasia (ADH) at 11:00 in the left breast (S21); and (f) a healthy subject with no breast nodules (S3).

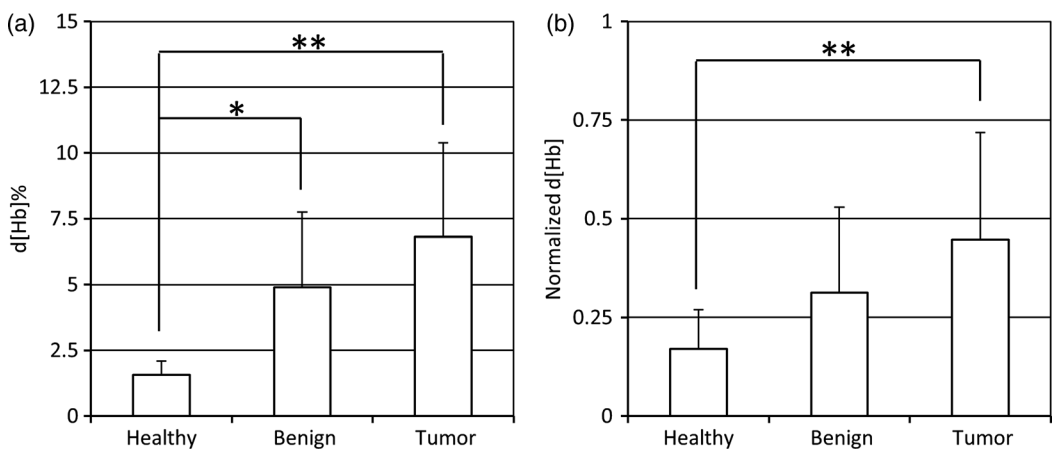

Fig. 5 Statistical analysis of the differences in Δ[Hb]% between healthy ($n = 6$), benign ($n = 8$), and tumor-bearing ($n = 14$) breasts 15 s after the end of a breath-hold. (a) Mean value and standard deviations of the average Δ[Hb]% in a 1-cm-sphere around the point of peak hemoglobin change. In (b), the Δ[Hb]% was normalized to the peak change in either breast over the course of the breath-hold for each patient. This provides a more uniform metric across patients. Error bars represent the standard deviation across subjects (*$p < 0.05$, **$p < 0.01$)

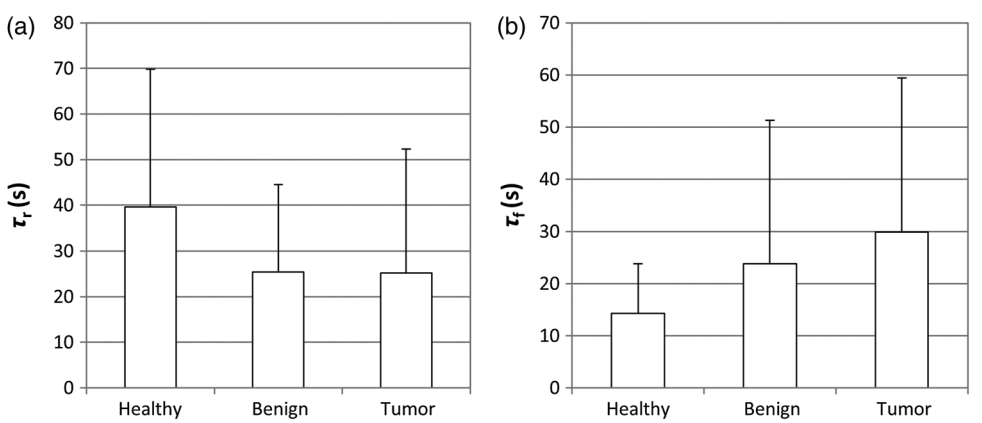

Fig. 6 Mean and standard deviations of the (a) rise-time (τ_r) and (b) fall-time (τ_f) constants for the exponential fit for healthy breasts ($n = 6$), breasts with a benign mass ($n = 8$), and breasts with a malignant mass ($n = 14$).

3.4 *Exponential Fitting of Breast Hemodynamics*

Finally, Fig. 6 shows the results of our statistical analysis concerning the fall and the rise times of the $\Delta[\mathrm{Hb}]\%$ signal when exponential functions are fitted [see Eq. (2)]. The average rise-time constant τ_r for the malignant tumor-bearing breasts ($\tau_r = 25.2$ s) appears to be smaller than for the healthy breasts ($\tau_r = 39.7$ s); however, because of the large standard deviation, the differences are not statistically significant ($p = 0.33$) [Fig. 6(a)]. The difference in the average fall-time constants between healthy and tumor-bearing breasts is more pronounced [Fig. 6(b)]. On average, healthy breasts have a faster washout rate ($\tau_f = 14.3$ s) compared with malignant-tumor-bearing breasts ($\tau_f = 29.9$ s) ($p = 0.09$), which agrees with the selection of the 15-s time point following the end of the breath-hold as a key time point for tumor visualization. The trends in uptake and washout rate provide insight into the hemodynamic responses of healthy and diseased tissues. A study with more healthy subjects and a larger number of breast cancer patients may shed more light on the significance of uptake and washout constants as biomarkers.

3.5 *False Negative and False Positive Cases*

In four tumor-bearing breasts, we were unable to visualize the tumor at the mid-recovery time point. Two of these cases (S6 and S13) involved large-breasted subjects with tumors near the chest wall. In these cases, it is possible that the fiber interface did not make adequate contact with the region of the breast that contained the tumor. As a result, the fiber interface was primarily imaging the healthy portion of the breast. In the third case (S16), suspicious nodules with tumor-like profiles were observed in the contralateral breast. These nodules were unbiopsied, so it is not clear how our finding relates to the pathology. In the fourth case (S14), the subject had very dense breasts, as indicated on the medical records.

In one of the breasts with a benign mass (S19), our imaging showed an enhancement in $\Delta[\mathrm{Hb}]\%$ in the location indicated by the medical records. The mass has not been biopsied, and the subject is scheduled for a follow-up visit in 6 months.

4 Discussion

4.1 *Origins of Dynamic Tumor Contrast*

In this study, we demonstrated that there are hemodynamic biomarkers of breast cancer that can be detected with dynamic optical tomography imaging during a breath-hold. Respiratory maneuvers, such as a breath-hold or valsalva maneuver, have been previously explored in brain DOT imaging, where an increased blood volume is observed in the region overlying valveless cerebral veins that experience hypertension during the respiratory maneuver.[34] While the effect of respiratory maneuvers is not well studied in the breast, increased blood volume has been reported in some case studies involving one to two patients using DOT imaging of the breast during a valsalva maneuver or breath-hold.[20,35] These respiratory maneuvers are believed to cause increased intrathoracic pressure that is transmitted through the vascular tree resulting in increased arterial and venous pressure.[36] In addition to the increased blood volume during the maneuver, these studies have also reported that the change in [Hb] in the breast appears to be more sensitive to respiratory maneuvers, similar to our observations.

The source of dynamic contrast comes from differences in the architecture and the structure between normal and tumor vasculatures. Growing tumors require increased vasculature in order to supply nutrients and oxygen, while also removing waste products from the expanding tumor. Once tumors surpass approximately 200 μm, the tumor cells can no longer rely on diffusion from the nearby vessels, and therefore must recruit new blood vessels by releasing proangiogenic growth factors. The newly formed vasculature is tortuous, disorganized, and hyperpermeable.[23] There are many shunts and stunted vessels that disrupt the normal artery-capillary-vein vascular hierarchy. Due to this disorganized structure, despite increased vasculature, the tumor perfusion remains poor. Poor perfusion combined with the high-metabolic activity of tumor cells causes tumors to be more hypoxic than the surrounding healthy tissue.[37]

In our study, the hemodynamic response of the tumor tissue differed from that of the healthy tissue. In healthy subjects, we saw a rise in [Hb] levels during the breath-hold, followed by a rapid return to the baseline levels upon the resumption of normal breathing. In tumor regions of the breast, we observed an increase in [Hb] levels during the breath-hold, followed by a much slower return to the baseline than in healthy subjects. We believe that this sluggish return to the baseline is due to the combined effect of the disorganized vasculature that affects blood flow in the tumor region and the hypoxic nature of oxygen-hungry tumors. Our results confirm and extend the results of case studies involving one or two patients looking at respiratory dynamics using DOT that reported a phase delay in the transient response of tumor tissue[17] and a sluggish recovery in [Hb] levels following a breath-hold.[20] Similar effects have also been seen in pressure-induced dynamic optical imaging, where an increased [Hb] is a hallmark of the tumor region during compression.[18]

4.2 *Study Limitations*

There are a number of clinical advantages of using dynamic DOT, which include the lack of compression during imaging, direct fiber contact with the breast which means no coupling fluid is required, and the use of endogenous contrast. The main disadvantage involves the variability in breath-holds performed by subjects. One of the four false negative subjects also suffered from asthma (S6), where poor breath-hold execution likely affected the DOT results. Asthma should be considered as a contraindication to future breath-hold studies.

Two subjects had large breasts (DDD and D size cups) with tumors located close to the chest wall (10 and 13 cm from the nipple). In those cases, we had difficulty in getting the tumor region into our optical breast interface due to the size of the breast, resulting in poor visualization of the tumor region. This issue can be addressed with more sophisticated designs for bringing the optical fibers in contact with the breast.

While this work included benign masses for analysis, its primary focus was in differentiating healthy tissue from malignant masses. Due to the variety of benign masses sampled and coupled with small sample size, it was not possible to infer strong statistical value from some of the benign subject data. While the work here shows some promising trends in the benign masses (typically falling in between healthy and malignant values), it is clear that a larger, more controlled study would be necessary to fully explore these findings.

5 Conclusions

We conducted a study exploring the hemodynamic changes in the breast during a breath-hold in 21 subjects (6 healthy breasts, 14 tumor-bearing breasts, and 8 breasts with benign masses). Using a newly designed dynamic DOT system that can acquire data simultaneously from both breasts at 1.7 Hz, we were able to analyze the transient response of the breast to a breath-hold. Healthy breasts showed an increase in [Hb] levels during the breath-hold, followed by a return to the baseline upon the resumption of breathing. In tumor-bearing breasts, the tumor region could be identified by its much slower recovery from the breath-hold. At a time point of 15 s following the end of the breath-hold, the tumor region can be visualized as an area of increased Δ[Hb]%, while the surrounding healthy tissue and contralateral breast show a fairly uniform return to the baseline values by that time point (healthy: $1.6\% \pm 0.5\%$; benign: $4.9\% \pm 2.7\%$; malignant: $6.8\% \pm 3.6\%$). Our analysis of the correlation between the Δ[Hb]% transient response in the left and the right breasts showed a high correlation in healthy subjects and in patients with benign masses and poorer correlation in subjects with malignant masses (healthy: 0.96 ± 0.02; benign: 0.89 ± 0.02; malignant: 0.78 ± 0.23). The fitting of an exponential function to the hemodynamics in the breast also showed that tumor-bearing breasts have different uptake and washout rates of deoxygenated hemoglobin. We believe that these findings reflect the effect of the disorganized tumor vasculature on the tissue hemodynamic response.

While these optical biomarkers appear to hold some promise in understanding the differences between benign and malignant masses, a larger, prospective study with more biopsied benign cases would be necessary to confirm the trends shown here. Overall, our study shows that dynamic optical markers have value in identifying breast tumors without the need for injected contrast agent, ionizing radiation, or painful compression. These findings provide a basis for analyzing transient responses for the detection of breast cancer in the hopes that this will provide another dimension for characterizing tumors to improve sensitivity, specificity, or better to predict tumor response to therapy.

Acknowledgments

We are grateful to all the patients who participated in this research. This study was supported in part by the Witten Family Fund and the New York State Office of Science, Technology and Academic Research—Technology Transfer Incentive Program (NYSTAR-TTIP: Grant No. #C020041) in collaboration with NIRx Medical Technologies. Molly Flexman was supported in part by the Natural Sciences and Engineering Research Council of Canada (NSERC). The authors would like to thank Dr. Randall Barbour and his laboratory at the State University of New York for their help in building the DOT instrumentation.

References

1. N. Howlader et al., *SEER Cancer Statistics Review, 1975–2008*, National Cancer Institute, http://seer.cancer.gov/csr/1975_2007/ (16 October 2011).
2. D. A. Berry et al., "Effect of screening and adjuvant therapy on mortality from breast cancer," *N. Engl. J. Med.* **353**(17), 1784–1792 (2005).
3. B. J. Tromberg et al., "Assessing the future of diffuse optical imaging technologies for breast cancer management," *Med. Phys.* **35**(6), 2443–2451 (2008).
4. R. Choe et al., "Differentiation of benign and malignant breast tumors by in-vivo three-dimensional parallel-plate diffuse optical tomography," *J. Biomed. Opt.* **14**(2), 024020 (2009).
5. L. C. Enfield et al., "Three-dimensional time-resolved optical mammography of the uncompressed breast," *Appl. Opt.* **46**(17), 3628–3638 (2007).
6. P. Taroni et al., "Time-resolved optical mammography between 637 and 985 nm: clinical study on the detection and identification of breast lesions," *Phys. Med. Biol.* **50**(11), 2469–2488 (2005).
7. S. van de Ven et al., "Diffuse optical tomography of the breast: preliminary findings of a new prototype and comparison with magnetic resonance imaging," *Eur. Radiol.* **19**(5), 1108–1113 (2009).
8. X. Intes, "Time-domain optical mammography SoftScan: initial results," *Acad. Radiol.* **12**(10), 934–947 (2005).
9. H. Rinneberg et al., "Detection and characterization of breast tumours by time-domain scanning optical mammography," *Opto-Electron. Rev.* **16**(2), 147–162 (2008).
10. J. Wang et al., "Near-infrared tomography of breast cancer hemoglobin, water, lipid, and scattering using combined frequency domain and CW measurement," *Opt. Lett.* **35**(1), 82–84 (2010).
11. A. Hagen et al., "Late-fluorescence mammography assesses tumor capillary permeability and differentiates malignant from benign lesions," *Opt. Express* **17**(19), 17016–17033 (2009).
12. H. Soliman et al., "Functional imaging using diffuse optical spectroscopy of neoadjuvant chemotherapy response in women with locally advanced breast cancer," *Clin. Cancer Res.* **16**(9), 2605–2614 (2010).
13. Q. Zhu et al., "Noninvasive monitoring of breast cancer during neoadjuvant chemotherapy using optical tomography with ultrasound localization," *Neoplasia* **10**(10), 1028–1040 (2008).
14. R. Choe et al., "Diffuse optical tomography of breast cancer during neoadjuvant chemotherapy: a case study with comparison to MRI," *Med. Phys.* **32**(4), 1128–1139 (2005).
15. M. G. Pakalniskis et al., "Tumor angiogenesis change estimated by using diffuse optical spectroscopic tomography: demonstrated correlation in women undergoing neoadjuvant chemotherapy for invasive breast cancer?," *Radiology* **259**(4), 365–374 (2011).
16. S. A. Carp et al., "Dynamic functional and mechanical response of breast tissue to compression," *Opt. Express* **16**(20), 16064–16078 (2008).
17. C. M. Carpenter et al., "Inspired gas-induced vascular change in tumors with magnetic-resonance-guided near-infrared imaging: human breast pilot study," *J. Biomed. Opt.* **15**(3), 036026 (2010).
18. L.S. Fournier et al., "Dynamic optical breast imaging: a novel technique to detect and characterize tumor vessels," *Eur. J. Radiol.* **69**(1), 43–49 (2009).
19. B. Wang et al., "Dynamic schema for near infrared detection of pressure-induced changes in solid tumors," *Appl. Opt.* **47**(16), 3053–3063 (2008).
20. C. H. Schmitz et al., "Design and implementation of dynamic near-infrared optical tomographic imaging instrumentation for simultaneous dual-breast measurements," *Appl. Opt.* **44**(11), 2140–2153 (2005).
21. X. Intes et al., "*In vivo* continuous-wave optical breast imaging enhanced with Indocyanine green," *Med. Phys.* **30**(6), 1039–1047 (2003).
22. R. X. Xu et al., "A prospective pilot clinical trial evaluating the utility of a dynamic near-infrared imaging device for characterizing suspicious breast lesions," *Breast Cancer Res.* **9**(6), R88 (2007).
23. R. A. Weinberg, *The Biology of Cancer, Garland Science*, Taylor and Francis Group, New York (2007).
24. M. L. Flexman et al., "Digital optical tomography system for dynamic breast imaging," *J. Biomed. Opt.* **16**(7), 1–14 (2011).
25. H. K. Kim et al., "PDE-constrained multispectral imaging of tissue chromophores with the equation of radiative transfer," *Biomed. Opt. Express* **1**(3), 812–824 (2010).
26. T. Durduran et al., "Bulk optical properties of healthy female breast tissue," *Phys. Med. Biol.* **47**(16), 2847–2861 (2002).
27. B. J. Tromberg et al., "Non-invasive measurements of breast tissue optical properties using frequency-domain photon migration," *Philos. Trans. Biol. Sci.* **352**(1354), 661–668 (1997).
28. Y. L. Pei, H. L. Graber, and R. L. Barbour, "Influence of systematic errors in reference states on image quality and on stability of derived

information for dc optical imaging," *Appl. Optic.* **40**(31), 5755–5769 (2001).
29. M. L. Flexman et al., "Monitoring early tumor response to drug therapy with diffuse optical tomography," *J. Biomed. Opt.* **17**(1), 016014 (2012).
30. C. H. Schmitz, H. L. Graber, and R. L. Barbour, "Peripheral vascular non-invasive measurements," in *Encyclopedia of Medical Devices, and Instrumentation*, J. G. Webster, Ed., pp. 234–252, John Wiley & Sons, Inc., New Jersey (2006).
31. S. Holm, "A simple sequentially rejective multiple test procedure," *Scand. J. Stat.* **6**(2), 65–70 (1979).
32. M. A. Seaman, J. R. Levin, and R. C. Serlin, "New developments in pairwise multiple comparisons: some powerful and practicable procedures," *Psychol. Bull.* **110**(3), 577–586 (1991).
33. S. A. Glantz, *Primer of Biostatistics*, 6th ed., pp. 101–105, McGraw-Hill, Medical Publishing Division, New York (2005).
34. A. Y. Bluestone et al., "Three-dimensional optical tomography of hemodynamics in the human head," *Opt. Express* **9**(6), 272–286 (2001).
35. R. L. Barbour et al., "Functional imaging of the vascular bed by dynamic optical tomography," *Proc. SPIE* **5369**, 132–149 (2004).
36. F. P. Tiecks et al., "Effects of the valsalva maneuver on cerebral-circulation in healthy adults: a transcranial Doppler study," *Stroke* **26**(8), 1386–1392 (1995).
37. P. Vaupel et al., "Oxygenation of human tumors: evaluation of tissue oxygen distribution in breast cancers by computerized O2 tension measurements," *Cancer Res.* **51**(12), 3316–3322 (1991).